lubricants

MDPI

Article

The Tribological Reduction Mechanism of the Rubber Hexagonal Surface Texture of the Screw Pump Stator

Zhongxian Hao [1,*], Songbo Wei [1], Deli Jia [1], Qinghai Yang [1], Xinglong Niu [2,*], Gang Zheng [3], Shijia Zhu [1] and Xinfu Liu [2]

[1] PetroChina Research Institute of Petroleum Exploration & Development, Beijing 100083, China
[2] School of Mechanical & Automotive Engineering, Qingdao University of Technology, Qingdao 266520, China
[3] China Petroleum Changqing Oil Field Company, Xi'an 710018, China
* Correspondence: haozx@petrochina.com.cn (Z.H.); nl18464268306@163.com (X.N.)

Abstract: This paper develops a composite weaving structure, combining hexagonal microbumps and hexagonal grooves, in the design of the rubber surface of the screw pump. This allows us to solve the problem of high torque and fast wear of the rubber stator during the operation of screw pump lifting oil recovery, based on the bionic hexagonal surface structure, traditional surface damping principle, and fluid dynamic pressure lubrication theory. Finite element analysis is first conducted to quantitatively analyze the impacts of the parallel side distance, groove width, and groove depth on the surface flow field and wall pressure field of the composite hexagonal structure. Based on the simulation law, the rubber surface laser structure is then designed and prepared by nanosecond laser processing. Afterward, tribological experiments are conducted under the condition of long-term immersion in the actual extraction fluid of shale oil wells. This aims at simulating the actual downhole oil production conditions and quantitatively studying the impact of the size of the composite hexagonal structure on the lubrication characteristics of the friction part of the stationary rotor, as well as the effect of abrasion reduction. The results show that, within the simulation range, the smaller the parallel side distance, the higher the load-carrying capacity. In addition, the hexagonal weave with a parallel side distance of 3 mm has a higher wall load carrying capacity than that with distances of 4 mm and 5 mm. When the groove width is equal to 0.4 mm, the oil film load carrying capacity is higher than that in the case of 0.2 mm. When the groove depth increases, the oil film pressure first increases and then stabilizes or decreases after reaching 0.3 mm. In the hexagonal weave, the friction ratio of the rotor is equal to 0.4 mm. In the tribological experiment of hexagonal weave, the smaller the parallel side distance, the smaller the friction coefficient, and the 0.5 mm weave has the highest performance.

Keywords: screw pump stator rubber; hexagonal texture; antifriction and resistance reduction; fluid lubrication

check for updates

Received: 9 December 2024
Revised: 14 January 2025
Accepted: 23 January 2025
Published: 27 January 2025

Citation: Hao, Z.; Wei, S.; Jia, D.; Yang, Q.; Niu, X.; Zheng, G.; Zhu, S.; Liu, X. The Tribological Reduction Mechanism of the Rubber Hexagonal Surface Texture of the Screw Pump Stator. *Lubricants* **2025**, *13*, 52. https://doi.org/10.3390/lubricants13020052

Copyright: © 2025 by the authors. Licensee MDPI, Basel, Switzerland. This article is an open access article distributed under the terms and conditions of the Creative Commons Attribution (CC BY) license (https://creativecommons.org/licenses/by/4.0/).

1. Introduction

More than 400,000 onshore production wells exist in China, supporting almost 200 million tons of crude oil output. They comprise more than 95% of artificial lifting wells. In addition, more than 98% of the crude oil-produced liquid comes from artificial lifting [1,2]. Using mechanical equipment to work on the fluid, energy is added to the bottom of the formation, and crude oil is extracted from the underground surface [3]. The basis of efficient oil well lifting is stable oil production and increase. The screw pump is stable, safe, and reliable, and it is the second-largest artificial lifting method. It is widely used in

general crude oil wells, as well as high-viscosity and high-sand-content oil wells [4–11]. In recent years, electric submersible screw pump rodless lifting has rapidly developed and has become a crucial important technical direction of platform well lifting. However, the relative movement between the rotors of the screw pump leads to friction and wear, as shown in Figure 1. According to the field application statistics of the electric submersible screw pump, more than 90% of the faults are caused by the wear and friction of the screw pump [12–14]. The main problems consist of the large friction torque and low efficiency of the wear pump. To prolong the operating life of the screw pump, many studies have been conducted on the friction performance of its stator bushing. For instance, Wang et al. [15] analyzed the form and characteristics of stator rubber wear under dry friction. Sun et al. [16] analyzed the wear types and characteristics of stator rubber at different positions. Liu et al. [17] studied the impact of the contact force and rotational speed on the friction and wear of the stator rubber using the method of friction and wear test. Han et al. [18,19] studied the impact of the interference quantity and friction coefficient on the stator wear of the screw pump.



Figure 1. Worn rubber stator of the screw pump.

In recent years, biomimetic surface engineering technology has been widely studied in the field of oil and gas engineering to reduce the friction between friction pairs. For instance, Guo et al. [20] presented a coupled PDC drill that mimics the surface structure of seashells using cellulose and lignin from bamboo as references, allowing an increase in drilling speeds by a factor of 1.5. The biomimetic surface texturing treatment has been studied according to the characteristics of biological surfaces in reducing resistance [21–26]. The application of surface texture technology on the surface of hard materials has also been studied, while studies on the application of soft materials, such as rubber, are still in their first stage. Some studies have shown that surface texture can also play a role in reducing friction on some soft materials. For instance, Yang et al. [27] studied the wear of rubber plates of propulsion bearings controlled by underwater vehicles. They compared the tribological properties of surface textured and non-textured rubber samples under the conditions of water lubrication, low speed, and overload. Their results showed that the friction coefficient and wear rate of surface textured rubber samples are reduced, which demonstrates that the surface texture reduces friction and increases wear resistance. Kasem et al. [28] made a surface texture for the rubber plunger surface of the syringe, which significantly reduced the friction resistance between the plunger and the tube wall. Zhang [29] prepared a surface texture on the stator rubber surface to improve its friction characteristics, allowing for reduced friction, extending the service life, and increasing work efficiency. Liu [30] mentioned that hexagonal grooves with centrosymmetric and axisymmetric features and an easy combination of multiple weaves can be used to reduce friction over the rubber in screw pumps. The anti-friction mechanism of surface texture on

hard materials has been studied, while the theoretical model on soft materials has not been studied yet [30–38]. After the development of the laser processing technology, more laser processing technologies are employed for surface texture processing [39–41]. Mao et al. discuss laser ablation, laser interference, and laser impact surface texturing processes for flexibility, very high processing accuracy, and good controllability for different conditions and materials [42].

Taking into consideration the actual application in the oil recovery site, in the case where the stator rubber of the screw pump has a large friction wear, causing pump failure, this study proposes to treat the surface texture of the rubber. This allows us to reduce the friction between the stator rubber and the rotor, and to increase the wear and abrasion resistance of the rubber. A dynamic pressure lubrication model of rubber contact fluid is developed, and a composite hexagonal texture, which combines micro-bumps and grooves, is designed and constructed. The distribution law of flow and pressure fields on the surface of high acrylonitrile rubber with a textured surface is also studied. In addition, tribological experiments are conducted to reveal the anti-friction mechanism of the surface texture on the surface of the soft material. By optimizing the surface texture dimensions and guiding the actual production in the field, the pump checking cycle of the screw pump well is extended and the production efficiency is increased.

2. Mathematical Model of the Dynamic Pressure Lubrication Theory

In this study, the following assumptions are made:

(1) Volumetric forces, such as gravity and magnetism, are not considered, and there is no relative sliding between the fluid surface and the solid interface.
(2) The fluid at the surface of the friction sub-surface is a Newtonian fluid of constant viscosity, regardless of the pressure variation in the direction of the film thickness.
(3) The screw pump stator and rotor between the soft and hard materials of the interference fit so that the contact surface is not completely in line contact, the surface of the weaving unit can be seen on the plane of contact, and the effect of the curvature of the oil film is negligible. The translational velocity is used instead of the speed of motion without taking the effect of the oil film curvature into consideration.
(4) The fluid flow on the surface of the friction pair is laminar, and the inertial forces are negligible compared with the viscous forces.
(5) In this paper, the selection of lubrication medium for low-viscosity shale oil with good fluidity is challenging, as it resists the viscosity changes even at a high shear rate. The viscosity is constant along the direction of the lubricant film thickness.

The Reynolds equation for the fluid on the surface of the weave (given by Equation (1)) [30]:

$$\begin{gathered}\frac{\partial}{\partial x}\left(\frac{\rho h^3}{\eta}\frac{\partial p}{\partial x}\right)+\frac{\partial}{\partial y}\left(\frac{\rho h^3}{\eta}\frac{\partial p}{\partial y}\right)= \\ 6\left[\frac{\partial}{\partial x}(U\rho h)+\frac{\partial}{\partial x}(V\rho h)+2\rho(w_{\mathrm{h}}-w_0)\right]\end{gathered} \tag{1}$$

where η is the fluid-viscosity, (Pa·s), p is the lubrication film pressure, (N), U, and V are the relative velocities of the friction pair along the x and y directions, and w_h and w_0 are the speeds of the two surfaces of the friction pair along the direction of the thickness of the lubrication film.

Neglecting the effect of pump temperature and pressure on viscosity and assuming that the viscosity in the fluid cell remains constant, the Reynolds equation for a locally pressurized fluid film can be written as (Equation (2)) [30]:

$$\frac{\partial}{\partial x}\left(\frac{\rho h^3}{\eta}\frac{\partial p}{\partial x}\right)+\frac{\partial}{\partial y}\left(\frac{\rho h^3}{\eta}\frac{\partial p}{\partial y}\right)=6U\frac{\partial}{\partial x}(\rho h) \tag{2}$$

Considering only the dynamic pressure effect term, the Reynolds equation can be simplified to the form presented in Equation (3) [33]. This can be used as Reynolds equation in the theoretical model of the lower surface texture of small gap where the incompressible fluid is dominated by laminar lubrication. Its form is given by:

$$\frac{\partial}{\partial x}\left(h^3\frac{\partial p}{\partial x}\right)+\frac{\partial}{\partial y}\left(h^3\frac{\partial p}{\partial y}\right)=6U\eta\frac{\partial h}{\partial x} \tag{3}$$

The bearing capacity of the plate can be obtained by integrating the surface pressure of the plate:

$$F_{\mathrm{W}}=\int_{\mathrm{A}}PdA \tag{4}$$

where P is the oil film pressure of the lubricating oil, (Pa), and A is the effective area between the plates, (m^2).

The friction force of the oil film can be obtained by integrating the shear stress on its surface:

$$F_{\mathrm{r}}=\int_{\mathrm{A}}\tau dA \tag{5}$$

where τ is the shear force of the lubricating oil film, (Pa).

The friction coefficient can be determined by calculating the bearing capacity and friction force of the lubricating oil film using Equations (4) and (5), respectively:

$$f=\frac{F_{\mathrm{r}}}{F_{\mathrm{w}}} \tag{6}$$

3. Fluid Simulation and Friction Experimental Analysis of Textured Surface

3.1. Simulation Model of Stator Inner Surface Texture

The surface texture geometric parameters mainly include the shape of the texture unit, parallel edge distance (D), groove width (w), and depth (h). Each parameter has its specific impact on the friction coefficient and lubrication state. Therefore, a reasonable selection of the surface texture parameters plays a crucial role in increasing the lubrication performance of the friction pairs. The scale of the snake can protect the body and reduce the friction resistance. In addition, the structure of the snake scale is hexagonal, and thus, in this study, the hexagonal surface texture is designed on the inner surface of the rubber stator of the screw pump with reference to the scale of the snake.

Figure 2 shows the three-dimensional model of the rubber surface texture of the stator of the screw pump. The finite element method and fluid analysis method are used to quantitatively analyze the impacts of different hexagon texture parallel edge spacing and texture groove width and depth on the friction properties of the friction pair of the screw pump fixed rotor.

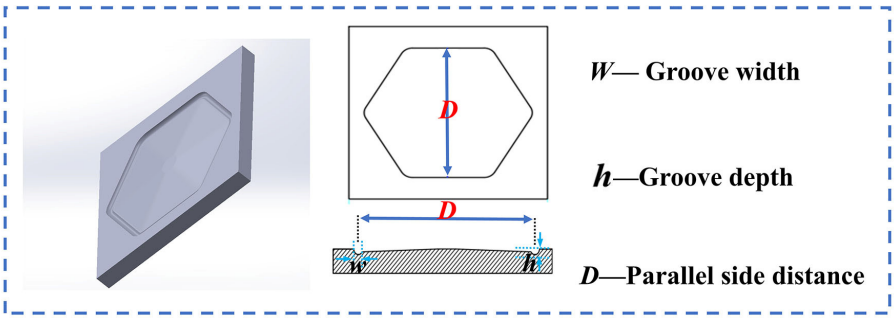


Figure 2. Geometric model of hexagonal surface textures.

The surface texture of the rubber sample of the screw pump stator was manufactured by nanosecond laser. The parallel edge spacing was set to 3, 4, and 5 mm, the groove width was set to 0.2 mm and 0.4 mm, and the groove depth was set to 10 μm, 50 μm, 100 μm, 200, and 300 μm. The impacts of the hexagon texture parallel edge distance, texture groove width, and texture depth on the friction properties were quantitatively analyzed.

The flow field and pressure field on the texture surface were analyzed using the finite element method according to the hexagonal texture geometry model. The three-dimensional fluid model was developed by finite element calculation on computational fluid dynamics (CFD) and fluid analysis software (Workbench 2020 R2 Fluent). The lubrication medium is selected from the actual extracted fluid from the shale oil production area in western China, having a viscosity of 0.08 mPa·s and 870 kg/m^3, and the lubrication weaving boundary condition is set to 101,325 Pa, with the flow rate set to 1 m/s.

The local encryption improves the mesh quality, as shown in Figure 3. When the number of meshes in the simulation model reaches 110 k, its impact on the calculation result is less than 5%.

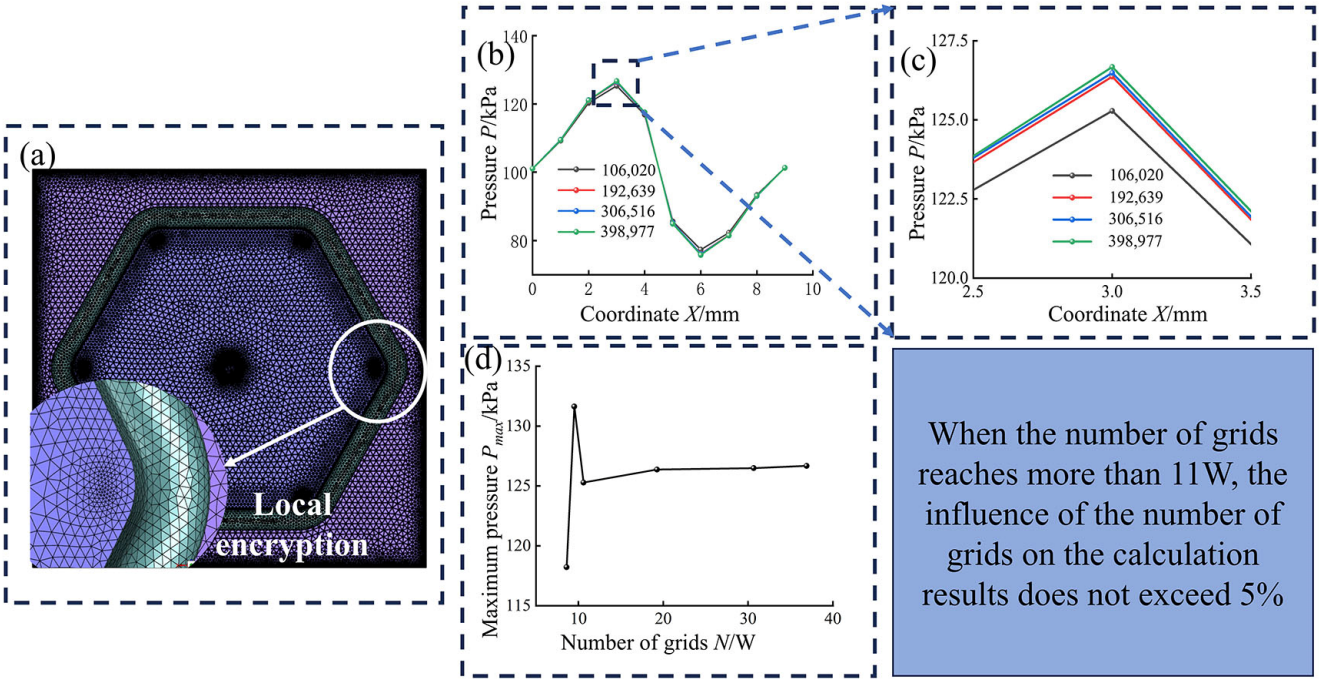


Figure 3. The meshed three-dimensional fluid model. (Fluid domain grid model (**a**), The surface pressure values are calculated under different grid numbers (**b**–**d**)).

3.2. Analysis of the Fluid Simulation Characteristics of the Texture Surface

Figure 4 shows the mean pressure cloud image of the oil film on the hexagonal surface with parallel edge margins of 3, 4, and 5 mm. It can be seen that the average pressure of the oil film on the upper wall with a parallel edge distance of 3 mm is higher, which indicates a higher bearing capacity.

Figure 4a,c show the pressure distribution on the upper surface of hexagonal textured oil film with different parallel edge distances. It can be seen that when the texture size increases, the fluid velocity inside the groove decreases, and its dynamic pressure effect decreases. Therefore, when the average pressure on the upper wall of the fluid decreases, the carrying capacity of the oil film also decreases.

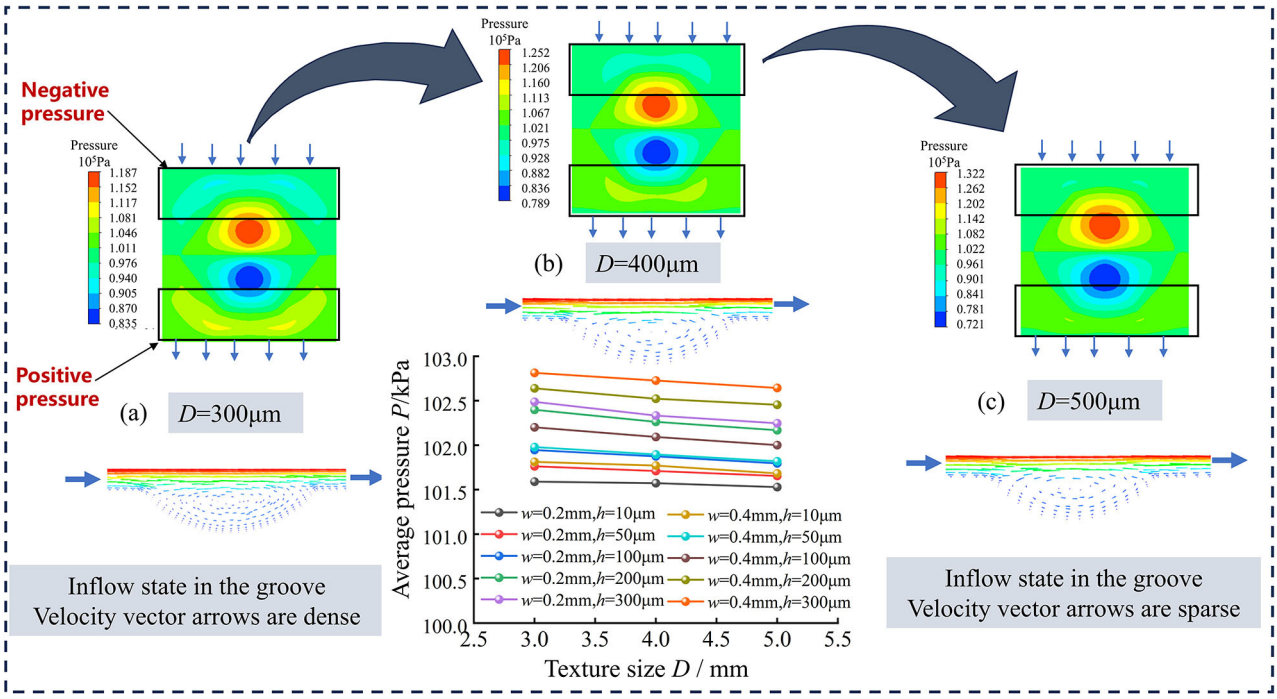


Figure 4. Mean pressure cloud image of the oil film on the groove of surface texture with parallel edge margins of 3 (**a**), 4 (**b**), and 5 mm (**c**).

It can be seen from Figure 5a that when the groove depth of the hexagonal texture increases, the average pressure on the wall of the oil film on the hexagonal texture surface first increases and then gradually stabilizes. The film pressure rapidly increases within the range of 300 μm, and the average pressure then stabilizes as the groove depth reaches 400 μm, and it finally decreases when the average pressure continues to increase.

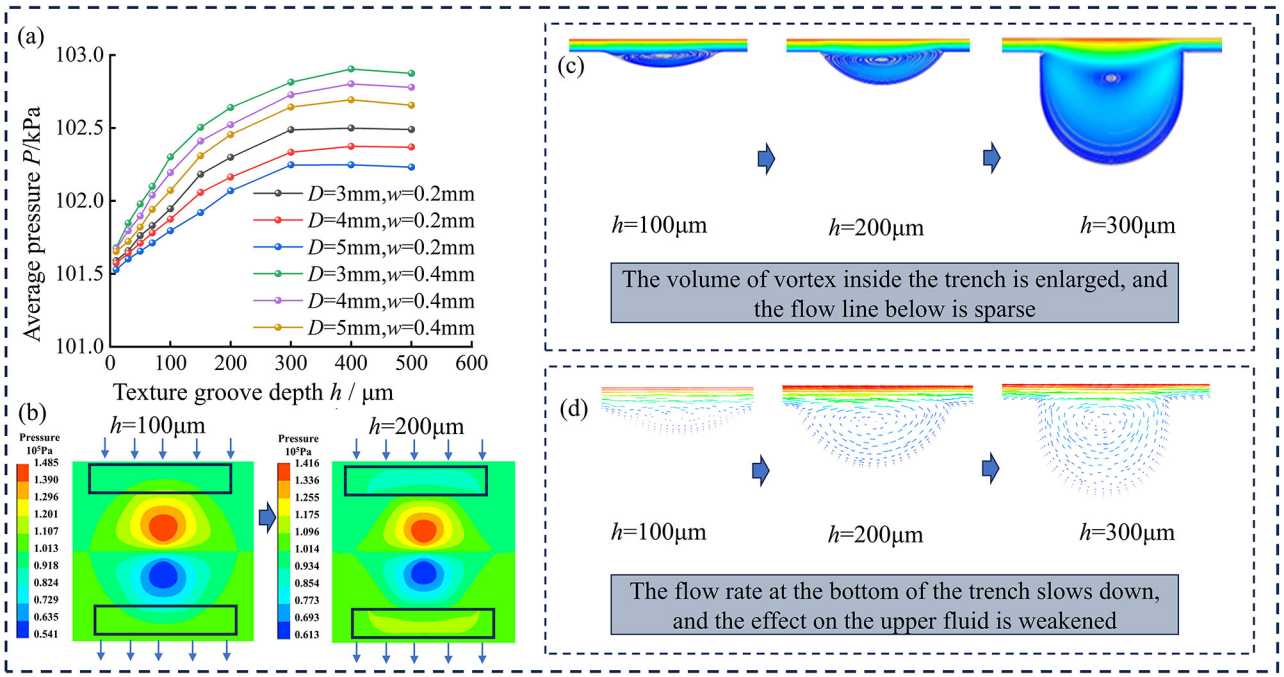


Figure 5. Texture groove pressure of the lubricating medium film function of the depth (As the groove depth changes, the pressure value (**a**), the pressure cloud image (**b**), the flow field (**c**) in the groove, and the velocity vector (**d**) change).

It can be observed from Figure 5b that when the depth increases, the positive and negative pressure zones vary, and the parallel edges of the positive pressure zones gradually tend to be equal. As a result, the additional bearing capacity obtained by the textured oil film decreases, and the average pressure reflected in the wall surface of the oil film also decreases. That is, the bearing capacity and the anti-friction effect both decreases.

It can be seen from Figure 5c,d that with the same groove width, when the groove depth increases, the fluid inside the groove forms a vortex. In addition, when the groove increases, the flow rate of its bottom decreases, and the impact on the upper fluid is reduced. Therefore, when the depth reaches 400 μm, the bearing capacity of the oil film first increases, and when the depth reaches 500 μm, it slowly decreases.

When the depth of the hexagonal textured grooves increases, the flow state at their location significantly changes. With a notch width of 0.4 mm, the texture groove starts to form vortices within at a depth of 100 μm. When the textured groove depth increases, the size of the vortices also increases. At a groove depth of 300 μm, the volume of the vortex reaches its maximum value. In this process, the greater the increase of the weaving depth, the greater the impact of the vortex on the upper fluid layer of the groove. In addition, the relative motion and viscous effect between the fluid layers produce vortex flow in the opposite direction of the upper layer of the fluid motion. Moreover, some of the reduced fluid kinetic energy is converted into vortex energy, and the energy loss caused by the vortex flow is increased compared with the previous process. The increase of the dynamic pressure lubrication effect of the wedge gap caused by the depth increase is not enough to offset the kinetic energy loss of the upper fluid due to the vortex generation. Thus, the average surface pressure first increases and then stabilizes or decreases when the depth at the weaving grooves continues to increase. The oil film-carrying capacity is higher at a groove width of 0.4 mm compared with that at 0.2 mm, which indicates higher lubrication performance. The composite hexagonal weave with a groove depth of 300 μm showed an average increase of 1.4% in the mean pressure on the wall of the grooves compared to the grooves with a depth of 10 μm, with a standard deviation of 0.00496.

3.3. Friction Experiment on Well Liquid Fabrication

In this experiment, the actual well fluid from a screw pump well in the oilfield is used. It belongs to a light crude oil with a paraffin base. The well fluid was pre-deaerated to remove the gas impact.

The surface texturing samples were manufactured on high-acrylic rubber by using a nanosecond laser, and the surface texture features of the sample were observed using the Olympus three-dimensional confocal microscope OLS500 (Olympus, Tokyo, Japan). Appropriate laser processing parameters were adopted to make the rubber surface texture clear. The processing parameters are shown in Table 1.

Table 1. Laser processing parameters.

Laser Processing Parameters	
Laser power	20 W
Engraving frequency	500 kHz
Engraving speed	800 mm/s
Number of engravings	5

The on-site conditions of the electric submersible screw pump show that the friction force of the rubber used in the pump will increase within a month. Therefore, the samples were immersed in actual well liquids at 70 °C for 31 days. The surface texture features are

shown in Figure 6. It can be clearly seen that after immersing tests, the surface textures still exist.

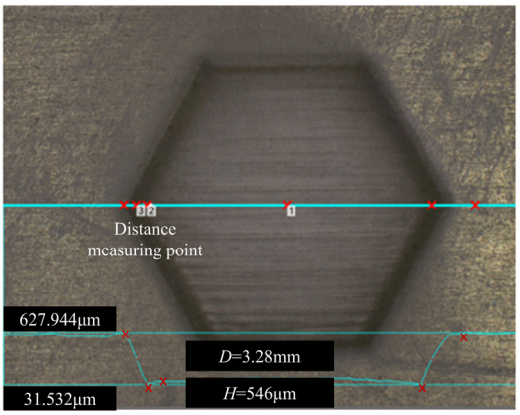


Figure 6. Hexagonal surface texture after immersing in actual well liquids at 70 °C for 31 days.

The friction experiment of the surface texturing samples after immersion was conducted using a UMT-3 reciprocating friction and wear tester, as shown in Figure 7a,c. The actual well liquids were used as a lubricating medium. The reciprocating frequency and travel were 3 Hz and 6 mm, respectively. A load of 30 N was used, and the experimental time for each sample was set to 900 s.

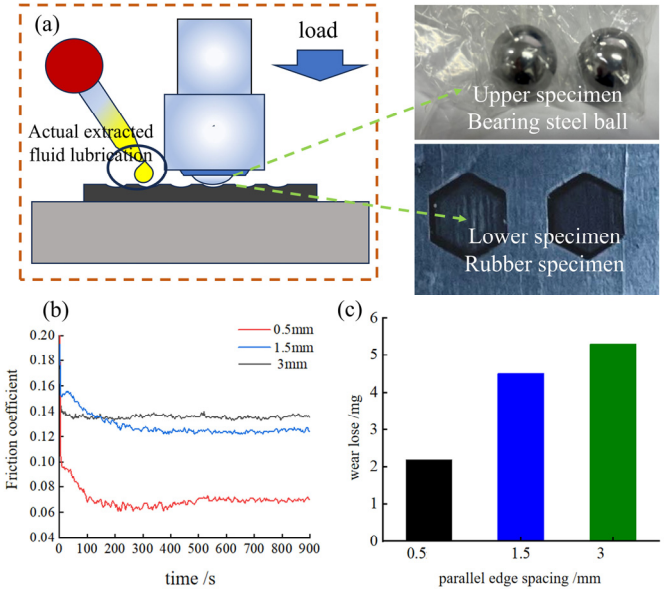


Figure 7. (**a**) Schematic diagram of the oil lubrication friction experiment, (**b**) friction coefficient, and (**c**) wear loss of hexagonal textures with parallel edge spacings of 0.5, 1.5, and 3 mm.

Figure 7a shows a schematic diagram of the friction and wear test process. As can be seen from Figure 7b,c, the hexagonal texture with parallel edge spacing of 0.5 mm has the smallest rubber friction coefficient and wear amount. When the parallel edge distance is equal to 3 mm, the friction coefficient and wear amount are the largest.

4. Conclusions

In this paper, the geometrical model of the hexagonal surface texture on the rubber of the screw pump stator was designed, and the mathematical model of the dynamic pressure lubrication of the textured surface was established. In addition, the impacts of the parallel edge distance, groove width, and depth on the dynamic pressure lubrication field on the

oil film-bearing capacity and friction characteristics were analyzed through theoretical analysis and conducted experiments.

The results show that the smaller the parallel spacing of the hexagonal micro texture in the study range, the greater the oil film pressure-bearing capacity. The parallel side spacing and width of the grooves were set to 3 mm and 0.4 mm, respectively. When the depth of the grooves increases, the average pressure of the oil film on the surface of the hexagonal texture first significantly increases and reaches its maximum value. Afterward, due to the increasing energy loss caused by eddy currents, the carrying capacity and anti-friction effect start to slowly decrease. A reasonable design of the hexagonal surface texture parameters can significantly increase the dynamic lubrication performance of the friction pair and the anti-friction wear performance of the stator rubber.

After 31 days of immersion in the actual well fluid at 70 °C, the surface texture of the rubber samples still exists. It is also observed that the smaller the spacing between the parallel edges of the hexagonal weave, the higher the load-bearing capacity and the friction and wear-reduction ability. The hexagonal texture of 0.5 mm exhibits the smallest rubber friction coefficient and the smallest wear.

Author Contributions: Conceptualization, Z.H., S.W., Q.Y. and X.L.; Methodology, Z.H., S.W., D.J., G.Z. and S.Z.; Software, Z.H., Q.Y. and X.N.; Validation, Z.H., S.W., D.J., X.N. and S.Z.; Formal analysis, Z.H., S.W., D.J., Q.Y., X.N. and S.Z.; Investigation, Z.H., S.W., D.J., Q.Y., X.N. and G.Z.; Resources, Z.H., Q.Y., G.Z. and X.L.; Data curation, Z.H., S.W., D.J. and G.Z.; Writing—original draft, Z.H., S.W., X.N. and S.Z.; Writing—review & editing, Z.H., S.W., X.N., G.Z. and X.L.; Visualization, Z.H., S.W., Q.Y. and S.Z.; Supervision, Z.H., D.J., Q.Y. and G.Z.; Project administration, Z.H., S.W., D.J. and X.L.; Funding acquisition, Z.H. and X.L. All authors have read and agreed to the published version of the manuscript.

Funding: This work was supported by the National Natural Science Foundation of China (Grant Nos. 52074161 and 52005281) and the Taishan Scholar Project of Shandong Province (Grant No. tsqn202211177).

Data Availability Statement: The original contributions presented in this study are included in the article. Further inquiries can be directed to the corresponding author.

Acknowledgments: The authors would like to thank the National Natural Science Foundation of China and CNPC for funding the project, CNPC for allowing me to share the paper, and all the teammates for supporting the experiment and calculation.

Conflicts of Interest: Authors Zhongxian Hao, Songbo Wei, Deli Jia, Qinghai Yang and Shijia Zhu were employed by the PetroChina Research Institute of Petroleum Exploration & Development. Author Gang Zheng was employed by the China Petroleum Changqing Oil Field Company. The remaining authors declare that the research was conducted in the absence of any commercial or financial relationships that could be construed as a potential conflict of interest.

References

1. Liu, H.; Hao, Z.; Wang, L.; Cao, G. Current technical status and development trend of artificial lift. *Acta Pet. Sin.* **2015**, *36*, 1441. [CrossRef]
2. Liu, H.; Liu, W.; Lu, Q.; Wang, S. Research status and development trend of deep well production technology. *J. Northeast Pet. Univ.* **2020**, *44*, 1–6+29+149.
3. Hao, Z.; Zhu, S.; Pei, X.; Peng, H.; Tong, Z.; Wang, B.; Li, D. Submersible direct-drive progressing cavity pump rodless lifting technology. *Pet. Explor. Dev.* **2019**, *46*, 621–628. [CrossRef]
4. Liang, Y.; Cao, G.; Shi, G.; Wang, G.; Li, J.; Zhao, Y. Progressing cavity pump anti-scaling techniques in alkaline-surfactant-polymer flooding in the Daqing Oilfield. *Pet. Explor. Dev.* **2011**, *38*, 483–490. [CrossRef]
5. Zhu, S.D.; Zhang, J.J.; Shi, J.F.; Liu, M.; Zhao, R.D.; Shu, Y. Research of Control System of Reciprocating Submersible Pump. *Oil Field Equip.* **2012**, *41*, 18–21.

6. Pozzi, N.; Bonfanti, M.; Mattiazzo, G. Mathematical modeling and scaling of the friction losses of a mechanical gyroscope. *Int. J. Appl. Mech.* **2018**, *10*, 1850024. [CrossRef]
7. Zhao, Z.; Ding, X.; Lookman, T.; Sun, J.; Salje, E.K.H. Mechanical loss in multiferroic materials at high frequencies: Friction and the evolution of ferroelastic microstructures. *Adv. Mater.* **2013**, *25*, 3244–3248. [CrossRef] [PubMed]
8. Antoni, G. On the mechanical friction losses occurring in automotive differential gearboxes. *Sci. World J.* **2014**, *1*, 523281. [CrossRef] [PubMed]
9. Peng, Y.G. Development and application of small displacement and high lift submersible direct drive screw pump. *Oil Field Equip.* **2022**, *51*, 83–88.
10. Han, D.Q.; Zhang, Y.; Song, Y.J. Lifting performance analysis of quasi-elliptical screw pump. *China Petrol. Mach.* **2021**, *49*, 132–137.
11. Li, X.F.; Gao, J.P.; Zhou, Z.Y. Effect of structural parameters on sealing performance of single screw pump. *China Pet. Mach.* **2011**, *39*, 72–74.
12. Wan, R.P. *Production Engineering Handbook*; Petroleum Industry Press: Beijing, China, 2003.
13. Jin, H.J.; Wu, H.A.; Cao, G.; Liu, H.; Wang, X.X. Slippage and abrasion mechanism of progressive cavity pump. *Eng. Mech.* **2010**, *27*, 179–184.
14. Oglesby, K.D.; Arellano, J.L.; Scheer, G. Fourteen years of progressing cavity pumps in a Southern Oklahoma waterflood. In Proceedings of the SPE Oklahoma City Oil and Gas Symposium/Production and Operations Symposium, Oklahoma City, OK, USA, 23–26 March 2003; p. SPE-80919. [CrossRef]
15. Wang, Z.; Wang, L. Research of friction and wear for stator rubber of oil extraction progressing cavity pump. *Mach. Des. Manuf.* **2014**, *2*, 163–166.
16. Sun, Y.P.; Qu, W.T.; Zhao, N.; Meng, D.X. Research on wear of stator of screw pump in CBM drainage. *Coal Technol.* **2017**, *36*, 222–224.
17. Liu, Z.H.; Tan, J.Z.; Liu, X.; Gao, X.Q.; Sun, J.B. Study on effects of contact force and rotational speed on friction and wear properties of screw pump stator material. *Fluid Mach.* **2019**, *47*, 1–6.
18. Han, C.J.; Ren, X.Y.; Zheng, J.P. Study on wear of stator bushing of conventional progressive cavity pump in heavy oil extraction. *Lubr. Eng.* **2018**, *43*, 25–29.
19. Han, C.J.; Ren, X.Y.; Zheng, J.P. Analysis of Abrasion for Stator Bushings of Equal Thickness Screw Pump in High Temperature and Sand Crude Oil. *China Mech. Eng.* **2017**, *28*, 446–450.
20. Guo, Y.; Zhang, Z.; Zhang, S. Advances in the application of biomimetic surface engineering in the oil and gas industry. *Friction* **2019**, *7*, 289–306. [CrossRef]
21. Liu, Z.; Yin, W.; Tao, D.; Tian, Y. A glimpse of superb tribological designs in nature. *Biotribology* **2015**, *1*, 11–23. [CrossRef]
22. Arslan, A.; Masjuki, H.H.; Kalam, M.A.; Varman, M.; Mufti, R.A.; Mosarof, M.H.; Quazi, M.M. Surface texture manufacturing techniques and tribological effect of surface texturing on cutting tool performance: A review. *Crit. Rev. Solid State Mater. Sci.* **2016**, *41*, 447–481. [CrossRef]
23. Chen, Y.; Wang, J.; Chen, M. Enhancing the machining performance by cutting tool surface modifications: A focused review. *Mach. Sci. Technol.* **2019**, *23*, 477–509. [CrossRef]
24. Wei, B.; Chen, W.; Guo, S.; Cheng, J.; Yuan, H.; Zhou, Y.; Luo, H.; Li, D. Study on the tribological characteristics of surface triangular textured TC4 alloy prepared by SLM technology. *Surf. Coat. Technol.* **2024**, *482*, 130735. [CrossRef]
25. Shi, Z.; Duan, X.; Chen, Z.; Liu, B.; Fu, H.; Ji, J.; Zhang, Y. Precision fabrication of micro-textures array for surface functionalization using picosecond pulse laser. *Opt. Laser Technol.* **2024**, *177*, 111200. [CrossRef]
26. Tian, S. *Study on the Effect of Surface Texture of Silicone rubber Insulator on Its Icing Performance*; China Three Gorges University: Yichang, China, 2020.
27. Yang, J.; Liu, Z.; Cheng, Q.; Liu, X.; Deng, T. The effect of wear on the frictional vibration suppression of water-lubricated rubber slat with/without surface texture. *Wear* **2019**, *426*, 1304–1317. [CrossRef]
28. Kasem, H.; Shriki, H.; Ganon, L.; Mizrahi, M.; Abd-Rbo, K.; Domb, A.J. Rubber plunger surface texturing for friction reduction in medical syringes. *Friction* **2019**, *7*, 351–358. [CrossRef]
29. Zhang, B.L. Study on Surface Texturing Flow Field Characteristics and Anti-friction Performance of Screw Pumped NBR. Ph.D. Thesis, Northeast Petroleum University, Daqing, China, 2021.
30. Liu, X.; Niu, X.; Liu, C.; Shi, X.; Sun, Y.; Hao, Z.; Huang, S.; Wang, Y.; Tao, H. Study on the Tribological Properties of Multilayer Concentric Hexagonal Laser Texturing on Rubber Surfaces of Screw Pumps. *Materials* **2024**, *17*, 3708. [CrossRef]
31. Zhang, B.L.; Zhao, L.X.; Liu, Y. Research progress in improving tribological properties based on surface texture technology. *Chin. J. Tribol.* **2021**, *42*, 202–224.
32. Liu, X.; Shi, X.; Hao, Z.; Wei, S.; Sun, Y.; Niu, X.; Li, Z. Effect of Complex Well Conditions on the Swelling and Tribological Properties of High-Acrylonitrile Stator Rubber in Screw Pumps. *Polymers* **2024**, *16*, 2036. [CrossRef] [PubMed]
33. Liu, X.; Sun, Y.; Liu, C.; Shi, X.; Niu, X.; Zheng, G.; Wei, W.; Wei, S.; Huang, S. Lubrication Characteristics of a Warhead-Type Irregular Symmetric Texture on the Stator Rubber Surfaces of Screw Pumps. *Lubricants* **2024**, *12*, 397. [CrossRef]

34. Wang, H.; Liu, Z.; Zou, L.; Yang, J. Influence of both friction and wear on the vibration of marine water lubricated rubber bearing. *Wear* **2017**, *376*, 920–930. [CrossRef]
35. Li, M.; Shi, W.; Shi, J.; Wang, T.; Shi, L.; Wang, X. Regulation and control of wet friction of soft materials using surface texturing: A review. *Friction* **2023**, *11*, 333–353. [CrossRef]
36. Wang, M.; Huang, Z.; Qian, W.; Li, G. Study of the effect of laser textured rotors on the starting performance of metal–rubber mating pairs under different lubricating media environments. *Proc. Inst. Mech. Eng. Part J J. Eng. Tribol.* **2024**, *238*, 450–463. [CrossRef]
37. Wang, M.; Li, Q.; Huang, Z.; Qian, W.; Chen, X.; Li, Q.; Lai, T. Influence of surface texture parameters of screw pump rotor on tribological properties of its friction pairs. *Ind. Lubr. Tribol.* **2022**, *74*, 964–974. [CrossRef]
38. Sahli, R.; Pallares, G.; Ducottet, C.; Ben Ali, I.E.; Al Akhrass, S.; Guibert, M.; Scheibert, J. Evolution of real contact area under shear and the value of static friction of soft materials. *Proc. Natl. Acad. Sci. USA* **2018**, *115*, 471–476. [CrossRef]
39. Convert, L.; Bourillot, E.; François, M.; Pocholle, N.; Baras, F.; Politano, O.; Costil, S. Laser textured titanium surface characterization. *Appl. Surf. Sci.* **2022**, *586*, 152807. [CrossRef]
40. Wu, X.F.; Zhan, J.M.; Mei, S.L. Optimization of micro-texturing process parameters of TiAlN coated cutting tools by femtosecond laser. *Materials* **2022**, *15*, 6519. [CrossRef]
41. Andersson, P.; Koskinen, J.; Varjus, S.; Gerbig, Y.; Haefke, H.; Georgiou, S.; Buss, W. Microlubrication effect by laser-textured steel surfaces. *Wear* **2007**, *262*, 369–379. [CrossRef]
42. Mao, B.; Siddaiah, A.; Liao, Y.L.; Menezes, P.L. Laser surface texturing and related techniques for enhancing tribological performance of engineering materials: A review. *J. Manuf. Process.* **2020**, *53*, 153–173. [CrossRef]

Disclaimer/Publisher's Note: The statements, opinions and data contained in all publications are solely those of the individual author(s) and contributor(s) and not of MDPI and/or the editor(s). MDPI and/or the editor(s) disclaim responsibility for any injury to people or property resulting from any ideas, methods, instructions or products referred to in the content.